Hindawi
Advances in Civil Engineering
Volume 2022, Article ID 1595651, 12 pages
https://doi.org/10.1155/2022/1595651

Research Article

Study on Environmental Effects Induced by Quasirectangle Shield Tunnelling with Analytical Stiffness Matrix

Jianguo Xu,[1] **Fengyang Miao**,[1] **Lei Kou**,[1] **and Jinpeng Zhang**[2]

[1]*School of Water Conservancy Engineering, Zhengzhou University, Zhengzhou 450001, Henan, China*
[2]*Henan Puze Expressway Company Limited, Puyang 457000, Henan, China*

Correspondence should be addressed to Lei Kou; klyhe@163.com

Received 4 January 2022; Accepted 21 March 2022; Published 9 April 2022

Academic Editor: Yonghong Wang

During the quasirectangle shield tunnelling, the soil around the tunnel is inevitably disturbed which results in different degrees of additional stresses and displacement of the soil. In this paper, the environmental effects caused by the construction of quasirectangle shield are analyzed by the analytical stiffness matrix method, focusing on the law of the additional stress field and the deformation of the multilayered soil induced by the construction of a quasirectangle shield. The results show that the additional stresses field has localized characteristics around the quasirectangle shield. The further away from the excavation face, the smaller the stress is. Also, shell friction and synchronous grouting pressure have a significantly greater influence on the additional stress field. Finally, the horizontal settlement groove of the quasirectangle shield is roughly symmetrical and parabolic along the tunnel axis, with a groove width range of about 20m. Synchronous grouting pressure has a greater effect on longitudinal ground deformation.

1. Introduction

With the gradual exploitation of underground space in the city, reasonable and efficient use is very important. In order to save the occupancy rate of urban underground space, civil engineers are constantly improving the construction process and proposing new construction technologies. The quasirectangle shield construction technology, which is based on the new structural section of the rectangular tunnel shield, is a new rail transportation construction technology. Compared to the rectangular shield tunnel, the main structure thickness of the quasirectangle shield tunnel is significantly reduced and the structural efficiency is higher. Compared to the circular shield tunnel, oval shield tunnel, and double circular shield tunnel, quasirectangle shield tunnel has higher section utilization rates. The quasirectangle shield tunnel takes up underground space decreased by 35% when the equivalent useable space is the same [1]. The buried depth of the quasirectangle shield tunnel is shallower, and the influence on the surrounding soil is slighter, which greatly improves the possibility of tunnelling through high-rise buildings or narrow roads.

Due to the influence of the shield tunneling to the ground, the soil is definitely disturbed, and the additional stresses are generated on the soil around the tunnel, which may cause ground settlement or uplift, resulting in different degrees of damage to the surface buildings and underground infrastructures [2, 3]. Scholars have paid more and more attention to the prediction of the effect on the building within the influence of the shield tunneling and how to control the ground settlement caused by tunnel excavation. The theoretical analysis of the additional stress field induced by the quasirectangular shield tunnel is mainly based on the Mindlin solution to establish the computational expressions for the additional thrust on the front side of the cutter, the frictional resistance between the shield shell and the soil, and the grouting pressure during the excavation of the shield tunnel in homogeneous stratum [4–7]. The research on ground settlement induced by quasirectangle shield tunneling is mainly based on Peck's formula and stochastic

medium theory to further deduces the formula for calculating and predicting ground settlement [6–9]. Existing literature on the environmental impact of tunnel construction has mostly focused on the analysis and prediction of soil deformation. Li et al. [10] proposed an analytical solution for the additional stresses in the curved tunnel based on Mindlin′s solution. Wu et al. [11] found that the friction force of the cutter head has little influence on the additional stress of the soil around the tunnel. Yuan et al. [12, 13] analyzed the displacement of layered soil through soil model tests and explored the effect of layer thickness on pile-soil interaction. Liang et al. [14] proposed a method based on the Pasternak foundation model and Mindlin′s solution to predict the impact of shield tunnel construction on nearby tunnels. Lai et al. [15] predicted soil deformation through artificial neural networks. Zhang et al. [16] considered the interaction mechanism between the tunnel liners and the surrounding soils and established a soil-liner interaction and nonuniform convergence model, which can predict the disturbed soil movements and tunnel liner deformation due to tunnel excavation. Zhao et al. [7] proposed the cut-off functions of ground surface settlement caused by double-O-tube tunnel shield construction. Wang et al. [17] provided a methodology for obtaining the analytical solutions of ground response induced by noncircular tunnel excavation. Zeng and Zuo [18] derived the theoretical solution of soil deformation considering the rolling of DOT shield by polar coordinate transformation and multi-subdomain integration method. Based on the virtual image technique, stress function solution and Bossiness's solution, Zou and Zou [19] proposed an elastic solution for the vertical nonaxisymmetric displacement boundary condition for the simultaneous grouting of the shield tunnel. Based on extreme gradient boosting and artificial neural network, Zhang et al. [20] established a prediction model to evaluate the surface settlement caused by EPB tunnel, which supports vector machine and multiple adaptive regression spline. However, natural strata exhibit multilayered properties during deposition, and the soil properties of different layers vary greatly. Existing studies usually simplify the complex multilayered problem to a homogeneous stratigraphic problem, which seldom considers the influence of the multilayered properties of the strata on the additional stress field and displacement of the soil around the tunnel induced by the shield tunnel construction.

This paper uses the analytical stiffness matrix method to analyze the additional stress field and displacement of the soil around the tunnel induced by the excavation of a quasirectangle shield in the multilayered soft soils, which is important theoretical guidance for determining the construction dynamic parameters of quasirectangle shield and protecting the safety of the buildings around the tunnel.

2. Analytical Stiffness Solution for the Loading of Multilayered Soil

Kou and Bai [21] deduced the unitary stiffness matrix for the three-dimensional spatial problem of laminar soil layer under loading in the Cartesian coordinate system.

$$K = \begin{pmatrix} k_{11} & \cdots & k_{14} \\ \vdots & \ddots & \vdots \\ k_{41} & \cdots & k_{44} \end{pmatrix}. \tag{1}$$

$$k_{11} = -\frac{2G\xi(2G+\lambda)\left[\left(1-e^{-4\xi z}\right)(\lambda+3G)+4\xi z e^{-2\xi z}(\lambda+G)\right]}{(\lambda+3G)^2\left(1+e^{-4\xi z}-2e^{-2\xi z}\right)-4\xi^2 z^2 e^{-2\xi z}(\lambda+G)^2}. \tag{1a}$$

$$k_{12} = \frac{2G\xi\left[4e^{-2\xi z}\xi^2 z^2(\lambda+G)^2-(\lambda+3G)G\left(1+e^{-4\xi z}-2e^{-2\xi z}\right)\right]}{\left(\lambda+3G^2\right)\left(1+e^{-4\xi z}-2e^{-2\xi z}\right)-4\xi^2 z^2 e^{-2\xi z}(\lambda+G)^2}. \tag{1b}$$

$$k_{13} = \frac{4G\xi e^{-\xi z}(2G+\lambda)\left[(3G+\lambda)\left(1-e^{-2\xi z}\right)+(G+\lambda)\left(1+e^{-2\xi z}\right)\xi z\right]}{(\lambda+3G)^2\left(1+e^{-4\xi z}-2e^{-2\xi z}\right)-4\xi^2 z^2 e^{-2\xi z}(\lambda+G)^2}. \tag{1c}$$

$$k_{14} = \frac{4G\xi^2 z e^{-\xi z}(2G+\lambda)(G+\lambda)\left(1-2e^{-2\xi z}\right)}{(\lambda+3G)^2\left(1+e^{-4\xi z}-2e^{-2\xi z}\right)-4\xi^2 z^2 e^{-2\xi z}(\lambda+G)^2}. \tag{1d}$$

$$k_{22} = \frac{2G\xi e^{-\xi z}(2G+\lambda)\left[(3G+\lambda)\left(e^{-4\xi z}-1\right)+4\xi z e^{-2\xi z}(G+\lambda)\right]}{(\lambda+3G)^2\left(1+e^{-4\xi z}-2e^{-2\xi z}\right)-4\xi^2 z^2 e^{-2\xi z}(\lambda+G)^2}. \tag{1e}$$

$$k_{24} = -\frac{4G\xi e^{-\xi z}(2G+\lambda)\left[(3G+\lambda)\left(e^{-2\xi z}-1\right)+(G+\lambda)\left(1+e^{-2\xi z}\right)\xi z\right]}{(\lambda+3G)^2\left(1+e^{-4\xi z}-2e^{-2\xi z}\right)-4\xi^2 z^2 e^{-2\xi z}(\lambda+G)^2}. \tag{1f}$$

$$\begin{aligned} &k_{21}=k_{12}, k_{23}=-k_{14}, k_{31}=k_{13}, k_{32}=k_{23}=-k_{14}.\\ &k_{33}=k_{11}, k_{34}=-k_{12}, k_{41}=k_{14}, k_{42}=k_{24}.\\ &k_{43}=k_{34}=-k_{12}, k_{44}=k_{22}, \end{aligned} \tag{1g}$$

where

$$\xi^2 = \xi_x^2 + \xi_y^2, \tag{1h}$$

$$\widetilde{f}\left(\xi_x,\xi_y,z\right) = \int_{-\infty}^{+\infty}\int_{-\infty}^{+\infty} f(x,y,z)e^{-i\xi_x x}e^{-i\xi_y y}dx\ dy, \tag{1i}$$

i is imaginary, G represents shear modulus, z is the depth of soil, λ describes the Lamé constant, K is the unit stiffness matrix of the plane strain problem for stratified strata subjected to load in the right-angle coordinate system, and the matrix elements of K are k_{11} and k_{12}.

The calculation model for the three-dimensional spatial problem of multilayered soil under loading is shown in Figure 1. According to the characteristics of the natural soil layer and calculation the foundation is divided into n layers, and H_i^- and H_i^+ are the vertical distances from the top and bottom of the layer i to the ground surface, and $\Delta h_i = H_i^+ - H_i^-$ is the thickness of the layer i. The applied load at the layer i is $q_i(x,y,z)$.

For the three-dimensional spatial problem of the multilayered soil under loading, at the surface of the foundation:

$$\sigma_x = \tau_{xz} = \tau_{yz} = 0, \tag{2}$$

At the base of the ground:

$$u = v = w = 0\,, \tag{3}$$

Assuming complete contact between adjacent calculation layers, the continuity condition for calculation layers without external load is as follows:

$$\begin{aligned} &M(\xi,H_i^+)=M(\xi,H_{i+1}^-), W(\xi,H_i^+)=W(\xi,H_{i+1}^-), N(\xi,H_i^+)=N(\xi,H_{i+1}^-).\\ &X(\xi,H_i^+)=X(\xi,H_{i+1}^-), Y(\xi,H_i^+)=Y(\xi,H_{i+1}^-), Z(\xi,H_i^+)=Z(\xi,H_{i+1}^-). \end{aligned} \tag{4}$$

The continuous conditions between the calculated layers with external load acting at $z = H_i$ are as follows:

$$\begin{aligned} &M(\xi,H_i^+)=M(\xi,H_{i+1}^-),\ W(\xi,H_i^+)=W(\xi,H_{i+1}^-), N(\xi,H_i^+)=N(\xi,H_{i+1}^-),\\ &X(\xi,H_{i+1}^-)=X(\xi,H_i^+)+q_{iX}(\xi,H_i), Y(\xi,H_{i+1}^-)=Y(\xi,H_i^+)+q_{iY}(\xi,H_i),\\ &Z(\xi,H_{i+1}^-)=Z(\xi,H_i^+)+q_{iZ}(\xi,H_i), \end{aligned} \tag{5}$$

where

$$\begin{aligned} &M=\frac{\xi_x\widetilde{u}+\xi_y\widetilde{v}}{\xi}, N=\frac{\xi_y\widetilde{u}-\xi_x\widetilde{v}}{\xi}, W=\widetilde{w}.\\ &X=\frac{\xi_x\widetilde{\tau_{xz}}+\xi_y\widetilde{\tau_{yz}}}{\xi}, Y=\frac{\xi_y\widetilde{\tau_{xz}}-\xi_x\widetilde{\tau_{yz}}}{\xi}, Z=\widetilde{\sigma_z}, \end{aligned} \tag{6}$$

where H_i^- and H_i^+, respectively, represent the depth of the upper and lower surfaces of the layer i; $q_{iX}(\xi,H_i)$, $q_{iY}(\xi,H_i)$, and $q_{iZ}(\xi,H_i)$ are the Fourier integral transformed load components acting at the i-th layer of soil.

Divide the natural layered ground into n calculation layers and apply the analytical element stiffness matrix to each calculation layer. By following the alignment principle of finite elements and combining it with the calculation of the continuous conditions between the layers, the overall analytic stiffness matrix for the three-dimensional spatial problem of the entire laminated foundation with loading can

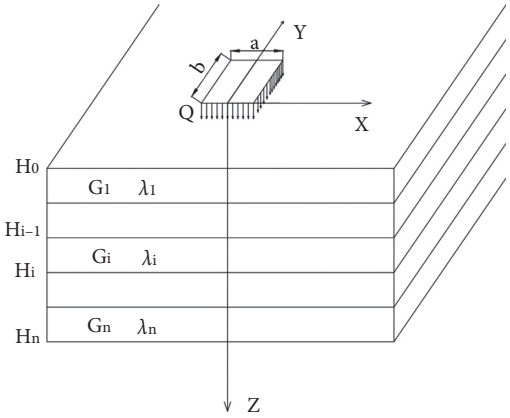

Figure 1: The calculation model of the three-dimensional spatial problem of layered stratum under loading.

be obtained, thus establishing the algebraic equations of stress and strain.

$$\begin{bmatrix} -Z(\xi,0) \\ -iX(\xi,0) \\ \vdots \\ -q_{iZ}(\xi,H_n) \\ -iq_{iX}(\xi,H_n) \\ \vdots \\ Z(\xi,H_n) \\ iX(\xi,H_n) \end{bmatrix} = \begin{bmatrix} K^{(1)} & & & & & & \\ & \ddots & & & & & \\ & & \ddots & & & & \\ & & & K^{(i)} & & & \\ & & & & \ddots & & \\ & & & & & \ddots & \\ & & & & & & K^{(n)} \end{bmatrix} \begin{bmatrix} W(\xi,0) \\ iM(\xi,0) \\ \vdots \\ W(\xi,H_i) \\ iM(\xi,H_i) \\ \vdots \\ W(\xi,H_n) \\ iM(\xi,H_n) \end{bmatrix}. \quad (7)$$

$$\begin{bmatrix} -Y(\xi,0) \\ \vdots \\ -q_{iY}(\xi,H_i) \\ \\ Y(\xi,H_n) \end{bmatrix} = \begin{bmatrix} K'^{(1)} & & \\ & K'^{(i)} & \\ & & K'^{(n)} \end{bmatrix} \begin{bmatrix} N(\xi,0) \\ N(\xi,i) \\ N(\xi,n) \end{bmatrix}. \quad (8)$$

In equations (7) and (8), $K^{(i)}$ and $K^{(i)}$ is the analytical stiffness matrix of layer i.

Combining the stress equation (7) and strain equation (8) to solve the stress and strain with boundary conditions, the solution to the three-dimensional space problem of the multilayered soil foundation under load in the Fourier integral transform domain can be obtained, and then invert the Fourier transform to derive the displacement component and stress in the real physical domain.

3. Model Analysis and Assumptions for Quasirectangle Shield

3.1. Overview of Quasirectangle Shield. As shown in Figure 2, without changing the basic geometry of the quasirectangle shield length, width, and height, the cross section of the quasirectangle shield is simplified to a combination of rectangular ABCD and two semicircles $\widehat{AECO_1}$ and $\widehat{BFDO_2}$. Compared with the actual geometry, the error of the frontal excavation area of the simplified model is 3.5%, and the error of the outer area of the shield shell is 1.5%, which is smaller and can meet the requirements of calculation accuracy.

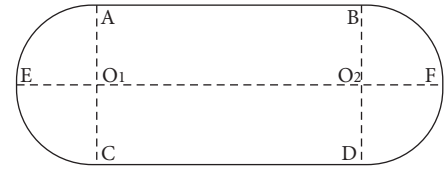

Figure 2: Cross section of the quasirectangle shield.

3.2. Analytical Models and Assumptions. An analytical model for quasirectangle shield tunneling in layer N is shown in Figure 3. Three types of interaction forces between the quasirectangle shield and the surrounding soil during the shield tunneling process are as follows: the additional thrust of the quasirectangle shield propeller to the soil q, the friction between the shell and the soil f, the synchronous grouting pressure p. The grouting pressure is not considered to be attenuated along the radial and longitudinal directions of the tunnel.

In order to calculate and analyze the magnitude and distribution of the additional stresses and displacements in the surrounding soil caused by the quasirectangle shield tunneling, the following assumptions were made:

(1) The quasirectangle shield machine excavated along the tunnel axis in a straight line, regardless of the influence of the shield deviation correction and rotation.

(2) Considering only the effects of shield excavation, the foundation is undrained during shield tunneling. When considering the influence of time changes, the foundation is drainage consolidation.

(3) According to the deposition process of a natural foundation, which is regarded as a semi-infinite space composed of n horizontal layers, each layer has a finite thickness and the soil in the layer is homogeneous and isotropic.

(4) The concentration of frontal additional thrust is q, the concentration of tunneling friction is f, and the concentration of grouting pressure is p. The directions of the frontal additional thrust, tunnelling friction, and grouting pressure are the direction of forces on the surrounding soil during shield tunneling.

4. Additional Stress for Quasirectangle Shield Tunnelling in Multilayered Soil

4.1. Additional Stress due to Additional Thrust on the Front of the Incision. As shown in Figure 2, the coordinates of the left semicircular excavation surface are as follows:

$$\left(0\ ,\ -\frac{K}{2}+r\cos\theta, h-r\ \sin\ \theta\right), \theta \in \left(\frac{\pi}{2},\frac{3\pi}{2}\right). \quad (9)$$

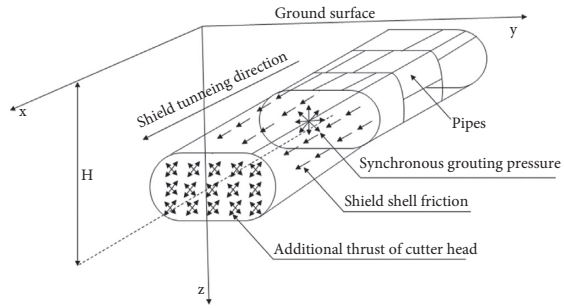

Figure 3: Analysis model of shield tunnel construction.

The coordinates of the right semicircular excavation surface are as follows:

$$\left(0\ ,\ \frac{K}{2}+rcos\theta, h-r\ \sin\ \theta\right), \theta\in\left(\frac{3\pi}{2},\frac{5\pi}{2}\right). \tag{10}$$

The coordinates of the middle rectangular partial excavation surface are $(0,\zeta,\eta)$. Integrating over the entire excavation surface, the additional stresses in the horizontal direction σ_x^1, σ_y^1 and the additional vertical stress σ_z^1 caused by the frontal additional thrust at any position in the soil (x,y,z) are as follows:

$$\sigma_x^1=\iint_{S_1} q\Omega(\xi,\zeta,\theta)r\ dr\ d\theta, \tag{11}$$

$$\sigma_y^1=\iint_{S_1} q\Psi(\xi,\zeta,\theta)r\ dr\ d\theta, \tag{12}$$

$$\sigma_z^1=\iint_{S_1} q\Phi(\xi,\zeta,\eta)r\ dr\ d\theta, \tag{13}$$

where S_1 is the area of the excavation surface of the shield tunneling, and its integration area is as follows:

$$x=0, H-\frac{D}{2}<z<H+\frac{D}{2}. \tag{14}$$

and

$$y=-\frac{K+D}{2}-\sqrt{\frac{D^2}{4}-(z-h)^2}\le y\le\frac{K+D}{2}+\sqrt{\frac{D^2}{4}-(z-h)^2}. \tag{15}$$

K is the width of the shield tunnel, D is the diameter of the shield; H is the depth of the tunnel center axis; $\Phi(r,\theta)$, $\Omega(r,\theta)$ and $\Psi(r,\theta)$ are, respectively, the z additional stress of x, y, z at any point in the soil caused by the unit frontal additional thrust, which can be calculated by the analytical stiffness matrix method.

The value of the frontal additional thrust q plays a key role in accurately calculating the magnitude of additional stresses and displacements in the foundation caused by the disturbance of the shield excavation [22]. In the existing studies, many researchers assume that the additional thrust force is 20 kPa, underestimating the additional stresses generated by the shield cutter squeezing the soil [23]. WANG et al. [24]believed that the soil squeezed by the shield was mainly composed of two parts: one was the pressure force on the excavated soil generated by the rotation of the cutter head, and the other was the squeezing force generated by the incision into the soil and proposed the frontal additional thrust q is calculated by the following:

$$q=\frac{10.13\pi(1-\nu)E_u v_t(1-\xi)^2}{(1+\nu)(3-4\nu)D_s k\omega}+\Delta q. \tag{16}$$

where Δq is the extrusion pressure generated by the shield cutter cutting the soil, generally 10 ~ 25 kPa; E_u is the elastic modulus of nondrainage of the soil (KPa) , which can be calculated by $E_u = E_s = 2.5 \sim 3.5E_{s0.1\sim0.2}$, ν is the Poisson's ratio of the soil, E_s is the elastic modulus of the soil, $E_{s0.1\sim0.2}$ is the compressive volume of the soil (MPa); v_t is the shield tunneling speed (cm/min); k is the number of closed portions of the cutter head; ω is the cutter rotational speed (rad/min), D_s is the cutter diameter, and ξ is the cutter opening ratio (%).

When constructing in multilayered soil, the additional frontal thrust should be calculated in layers due to the differences of the soil properties in each layer.

4.2. Additional Stresses due to Frictional Resistance in Tunnelling. As shown in Figure 2, pick any tiny unit on the contact surface between the shield shell and the ground. The unit area is $D\ d\ l\ d\theta/2$, where the tunneling friction is $f\ Dd\ l\ d\theta/2$, f is the trenching frictional resistance load, D is the shield diameter, and l is the integration parameter of the shield machine in the excavation direction. The additional stress in the horizontal direction σ_x^2, σ_y^2 and the additional vertical stress σ_z^2 caused by the frictional resistance between the shield shell and the soil during shield tunneling at any position in the soil (x,y,z) are as follows:

$$\sigma_x^2=\iint_{S_2} f\ D\Omega\frac{(l,\theta)}{2}dl\ d\theta. \tag{17}$$

$$\sigma_y^2=\iint_{S_2} f\ D\Psi(l,\theta)/2\ dl\ d\theta \tag{18}$$

$$\sigma_z^2=\iint_{S_2} f\ D\Phi\frac{(l,\theta)}{2}dl\ d\theta, \tag{19}$$

where S_2 is the side area of the shield shell in contact with the soil; its integration area is as follows:

$$-L\le x\le 0, H-\frac{D}{2}\le z\le H+\frac{D}{2},$$

$$-\frac{K+D}{2}-\sqrt{\frac{D^2}{4}-(z-h)^2}\le y\le\frac{K+D}{2}+\sqrt{\frac{D^2}{4}-(z-h)^2}, \tag{20}$$

L is the length of the shield. $\Phi(r,\theta)$, $\Omega(r,\theta)$ and $\Psi(r,\theta)$ are, respectively, the additional stress of z, x, y at any point in the soil caused by the unit frictional resistance of the excavation, which can be calculated by the analytical stiffness matrix method.

The frictional resistance of the excavation at any position on the contact surface between the shield shell and the ground soil is calculated by the formula for the frictional resistance between the pile and the soil proposed by ALONSO et al. [25].

$$f = \tau_{sr} = \beta_s \sigma_\theta \tan\delta, \tag{21}$$

where σ_θ is the positive radial stress acting on the shield shell,

$$\sigma_\theta = \sigma_v \sin^2\theta + \sigma_h \cos^2\theta, \tag{21a}$$

σ_v, σ_h is the vertical and horizontal ground soil pressure,

$$\sigma_h = K_0 \sigma_v, \tag{21b}$$

$$\sigma_v = \gamma H - \gamma D \sin\frac{\theta}{2}, \tag{21c}$$

K_0 is the horizontal static soil pressure coefficient; δ is the friction angle between the shield shell and the surrounding soil body, which can be obtained through the interfacial shear test.

4.3. Additional Stresses due to Grouting Pressure. As shown in Figure 3, pick a tiny unit in the tunnel surface, the unit area is $D\,d\,s\,d\theta/2$, the grouting pressure on the unit area is $p\,Dd\,s\,d\theta/2$, in which p is the grouting pressure load, s is the integration parameter of grouting in the excavation direction. The additional stresses in the horizontal direction σ_x^2, σ_y^2 and the additional vertical stress σ_z^2 caused by the grouting pressure of the shield construction are as follows:

$$\sigma_x^3 = \iint_{S_3} p\,D\Omega\frac{(s,\theta)}{2}ds\,d\theta, \tag{22}$$

$$\sigma_y^3 = \iint_{S_3} p\,D\Psi\frac{(s,\theta)}{2}ds\,d\theta, \tag{23}$$

$$\sigma_z^3 = \iint_{S_3} p\,D\Phi\frac{(s,\theta)}{2}ds\,d\theta, \tag{24}$$

where S_3 is the area where the grouting pressure acts, and its integral area is as follows:

$$-L - s \le x \le -L, \tag{25}$$

$$H - \frac{D}{2} \le z \le H + \frac{D}{2}, \tag{26}$$

$$-\frac{K+D}{2} - \sqrt{\frac{D^2}{4} - (z-h)^2} \le y \le \frac{K+D}{2} + \sqrt{\frac{D^2}{4} - (z-h)^2}, \tag{27}$$

s is the grouting length; $\Phi(r,\theta)$, $\Omega(r,\theta)$ and $\Psi(r,\theta)$ are, respectively, the additional stress of z, x, y at any point in the soil caused by the grouting pressure of the shield construction, which can be calculated by the analytical stiffness matrix method.

4.4. Total Additional Stress of Soil. Adding the additional soil stresses caused by the additional frontal thrust, shield shell friction, and grouting pressure, the total additional stresses in the soil caused by the construction of the quasirectangle shield are obtained.

$$\sigma_x = \sigma_x^1 + \sigma_x^2 + \sigma_x^3, \tag{28}$$

$$\sigma_y = \sigma_y^1 + \sigma_y^2 + \sigma_y^3, \tag{29}$$

$$\sigma_z = \sigma_z^1 + \sigma_z^2 + \sigma_z^3, \tag{30}$$

5. Displacement for the Quasirectangle Shield Tunnelling in Multilayered Soil

The displacements of the foundation were caused by the stratum loss and soil disturbance when the shield was excavated. In this paper, the analytical stiffness matrix method is used to calculate the displacements caused by the quasirectangle shield tunnel construction in multilayered soil.

According to equations (2) to (6), we can get the following:

$$\begin{aligned} \widetilde{u} &= \frac{\xi_x M + \xi_y N}{\xi}, \\ \widetilde{v} &= \frac{\xi_y M - \xi_x N}{\xi}, \\ \widetilde{w} &= W(\xi, H_i). \end{aligned} \tag{31}$$

$$\begin{aligned} \widetilde{u}_i &= \frac{iM(\xi,H_i)\xi_x + N(\xi,i)\xi_y}{\xi}, \\ \widetilde{v}_i &= \frac{iM(\xi,H_i)\xi_y - \xi_x N(\xi,i)}{\xi}, \\ \widetilde{w}_i &= W(\xi,H_i). \end{aligned} \tag{32}$$

Use the inverse Fourier transform to obtain the displacement of each soil layer and the sum of the displacement of each soil layer to obtain the entire stratum displacements during the Quasirectangle Shield tunneling.

$$u = \sum_{1}^{n} \widetilde{u}_i, v = \sum_{1}^{n} \widetilde{v}_i, w = \sum_{1}^{n} \widetilde{w}_i. \quad (33)$$

where u and v are the deformations of the soil layer in the horizontal direction, w is the settlement of the soil layer in the vertical direction.

6. Project Examples and Discussion

6.1. Project Overview. The shield of the Ningbo Metro Line 3 used a quasirectangular Earth pressure balance shield machine made in China for construction. The dimension of the shield machine is shown in Table 1.

The soil layers traversed by the shield tunnel mainly consist of Sludge ④ and Sludge-Clay ⑤, and the main physical and mechanical properties of each layer are shown in Table 2.

Several monitoring sections are arranged along the tunnel axis in this project. In view of the soil disturbance and deformation caused by the quasirectangle shield construction, this paper uses the 241st ring monitoring section data for comparative analysis. The surface elevation of the section is 2.6 m, the center elevation of the tunnel is -8.581 m, and the buried depth of the tunnel axis is 11.2 m. According to the method proposed in Sections 2 and Sections 4, the additional stress on the ground caused by the disturbance of the shield construction is calculated.

6.2. Additional Stress Analysis

6.2.1. Comparison with Monitoring Data. The comparison between the calculated value and the monitoring data of the additional stress σ_x and σ_y of the soil above the tunnel axis when the shield machine arrived the 241st ring, as shown in Figure 4. Along the direction of buried depth of the tunnel, the distribution pattern of the calculated values of σ_x and σ_y is consistent with the monitoring data. Since the theoretical analysis cannot fully simulate the actual situation, there are some differences between the theoretically calculated values and the actual engineering measurements, but the differences are small. Therefore, the distribution pattern of the calculated values of σ_x and σ_y can provide a theoretical basis for discussing the additional stresses in the soil around the tunnel caused by the quasirectangle shield.

6.2.2. Additional Stress σ_x. Figure 5 shows the distribution of additional stresses σ_x induced by additional frontal thrust, shell frictional resistance, and grouting pressure at 6 m above the tunnel axis from the surface ($y = 0$, $z = 6$). The additional stress σ_x is approximately distributed antisymmetrically along the central axis of the shield tunnel. During the shield tunneling, the front soil is under pressure, and the pressure reaches the maximum at the position 5 m in front of the excavation; the back soil is under tension, and the tension reaches the maximum at the shield tail position. Frontal additional thrust and shell frictional resistance affect σ_x similarly due to their different positions of action. Their antisymmetric points do not coincide. Compared with the frontal additional thrust and synchronous grouting pressure, the shell friction has a greater effect on σ_x, so that the additional stress distribution curve caused by three together is close to the additional stress distribution curve caused by the shell friction.

The distribution of the additional stress σ_x along the X-axis is shown in Figure 6. σ_x is approximately antisymmetric along the shield direction, and the front and back influence range of $y = d$ is roughly -25m ~ 25 m. During the shield tunneling, the soil at the front of the shield is compressed, and the maximum value of σ_x is concentrated at 5m in front of the shield, and the soil at the middle and back of the shield is under tension, and the maximum value of σ_y is concentrated on the tail of the shield. As the distance from the excavation surface increases, the additional stress value gradually decreases. Obviously, the additional stress σ_x hardly changes in the range $y = 0$ to $y = d$, and the additional stress σ_x increases significantly in the range $y = d$ to $y = d + R_1$.

Figure 7 illustrates the distribution of σ_x along the Y axis. σ_x is distributed symmetrically about the tunnel axis, and the influence range of σ_x is 20 m away from the shield axis. The farther away from the shield axis, the additional stress will be smaller and the attenuation will be slower. About 10 m away from the tunnel axis, the additional stress changes little and the curve is relatively flat, indicating that due to the quasirectangle shield, the extrusion range of the front soil is concentrated within the width of the shield.

6.2.3. Additional Stress σ_y. Figure 8 shows the distribution of additional stresses σ_y induced by additional frontal thrust, shell frictional resistance, and grouting pressure at 6 m above the tunnel axis from the surface. The frontal additional thrust and shell friction have similar effects on σ_y, both of which make the soil at the front of the shield laterally compressed, and the soil at the back is laterally undertension. Under the grouting pressure, the lateral tension on the soil above the tunnel axis is greater and reaches a maximum at the tail position of the shield. Obviously, the effect of synchronous grouting pressure on σ_y is much greater than the effect of additional thrust and shell frictional resistance, resulting in σ_y distribution curve similar to that of σ_y when synchronous grouting acts alone. Thus, synchronous grouting, the grouting volume, and slurry pressure shield tunneling should be strictly controlled.

As can be seen from Figure 9, the distribution of additional stresses σ_y before and after excavation varies greatly and depends on the distance from the excavation surface. At the tail of the shield, the additional stress σ_y suddenly changes to the maximum. Locations near the excavation surface, the front of the excavation is in lateral compression with additional stresses reaching a maximum. and the back of the excavation is in lateral tension. σ_y is mainly affected by synchronous grouting pressure.

It can be seen from Figure 10 that σ_y presents the symmetrical distribution of "arches" on the shield axis. The soil directly in front of the excavation surface is obviously squeezed. The value of σ_y is larger at a certain distance before

Table 1: The dimensions of the quasirectangle shield machine.

Shield width K/m	Shield height H/m	Shield length L/m	Shield radius R/m
11.83	7.26	11.61	3.37

Table 2: Main physical and mechanical properties of the soil layer.

No.	Soil layer	Soil thickness = / m	Gravity/ KN·m3	Compression modulus/ MPa	Poisson's ratio	Static side pressure coefficient K0
1	Miscellaneous soil	1.50	18.0	3.41	0.38	0.60
2	Sludge	1.70	16.4	1.65	0.42	0.72
3	Clay	0.80	18.3	3.15	0.37	0.63
4	Sludge	4.40	16.5	1.63	0.42	0.72
5	Sludge-clay	8.40	17.2	2.02	0.40	0.67
6	Silt-clay	3.70	18.3	3.03	0.32	0.47
7	Sludge-silt-clay	7.30	18.0	2.84	0.35	0.54
8	Clay	5.70	17.4	3.87	0.35	0.55

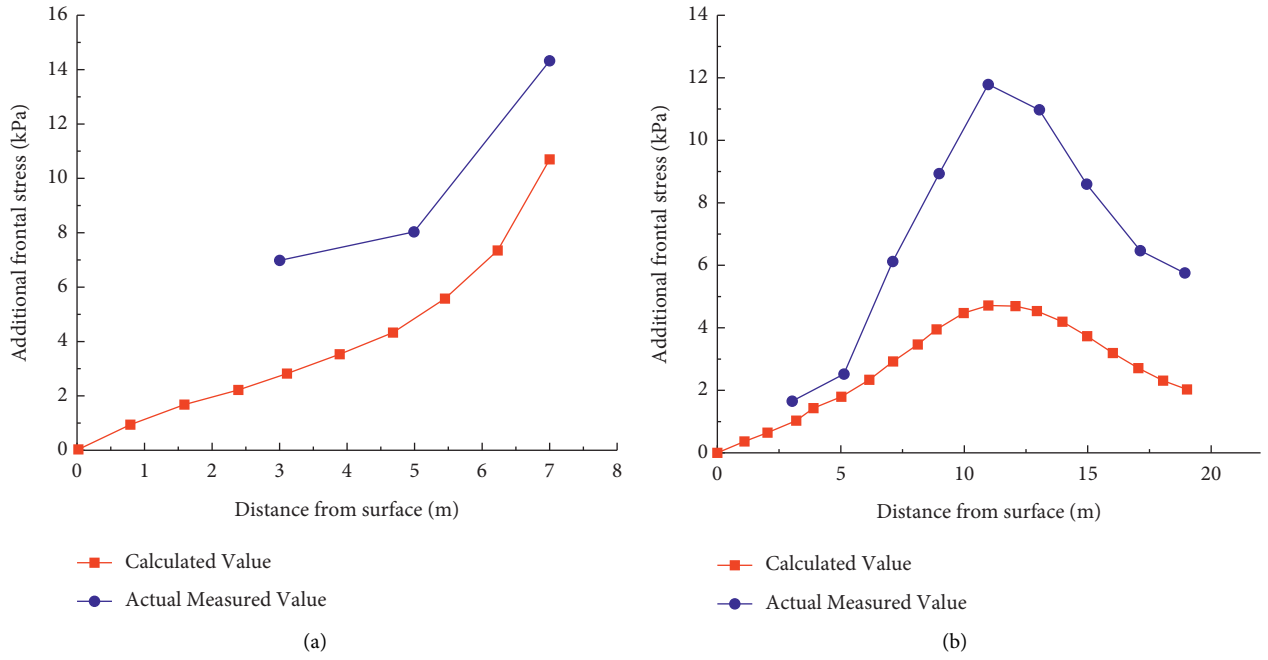

Figure 4: Comparison of calculated and monitoring data of σ_x (a) and σ_y (b).

excavation and the maximum value is located at the shield axis. As the distance from the excavation surface gets farther and farther, the peak point gradually moves to both sides of the shield, the additional stress spread tends to slow down, and the stress tends to be evenly distributed.

6.3. Displacement Analysis

6.3.1. Comparison with Monitoring Data. The comparison between the theoretical value of the lateral displacement of the soil and the monitoring data of the inclined tube CX-241-2 when the shield reached the 241st ring is shown in Figure 11. The monitoring of horizontal displacement fluctuates greatly. As the theoretical analysis cannot fully simulate actual construction which is influenced by many factors, the monitoring data is smaller than the calculated value, but the trends of the two are similar. The horizontal and longitudinal deformation patterns of the surface obtained in this paper can provide some theoretical basis for reducing the surface deformation caused by quasirectangle tunneling.

6.3.2. Horizontal Displacement. Figure 12 shows the theoretical value of the horizontal displacement of the soil at the side inclined tube CX-241-2 when the shield reached the 241st ring, which is located on the right side of the tunnel in the forward direction and which has a horizontal distance of about 1.25 m ($y = 7$ m) from the tunnel. The additional

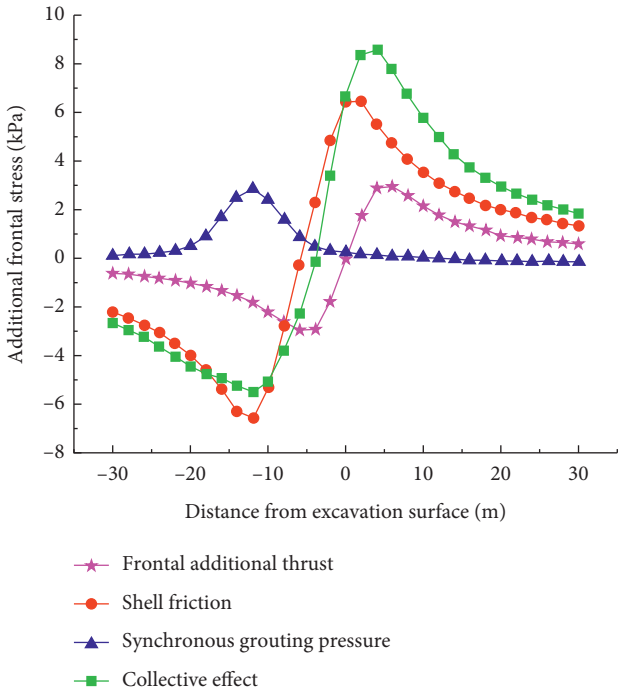

Figure 5: The effect of additional frontal thrust, shell frictional resistance, and synchronous grouting force on σ_x.

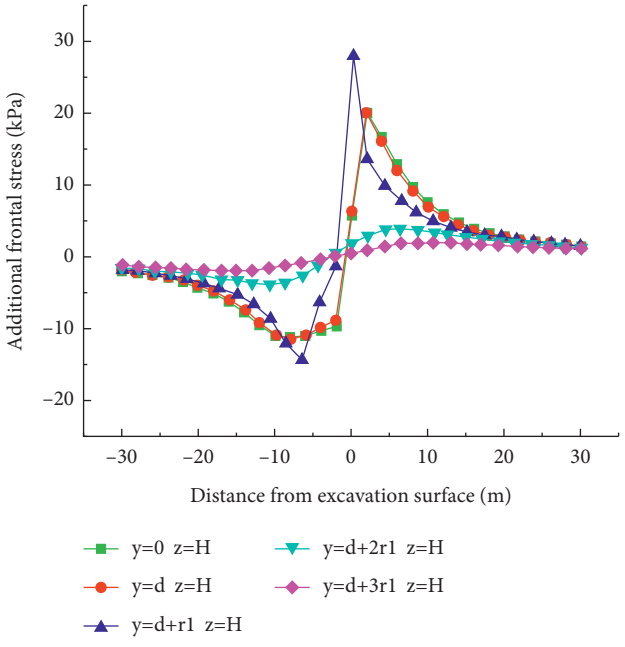

Figure 6: The distribution of the additional stress σ_x along the X axis.

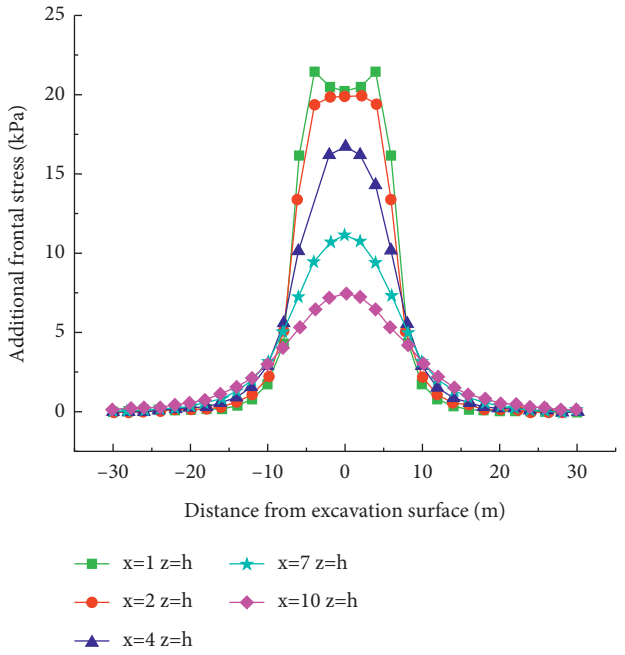

Figure 7: The distribution of the additional stress σ_x along the Y axis.

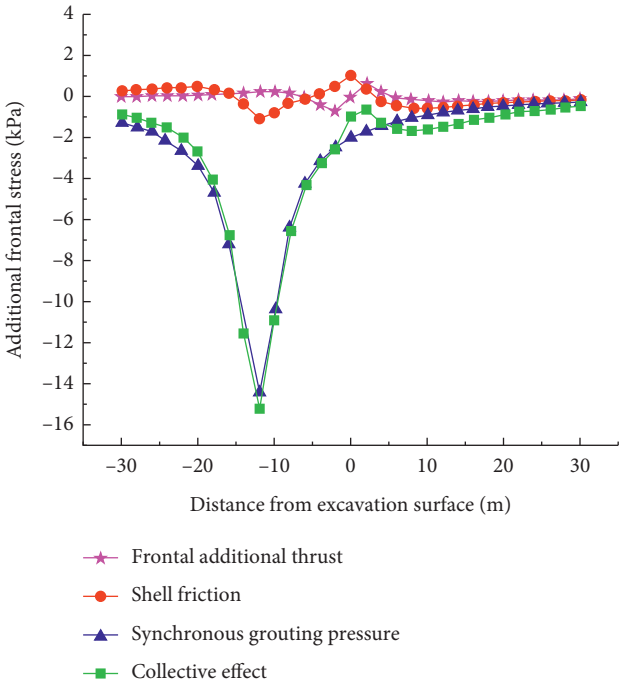

Figure 8: The effect of additional frontal thrust, shell frictional resistance, and synchronous grouting force on σ_y.

frontal thrust acts on the position $x = 0$, and the horizontal displacement is $v = 0$. Therefore, when the shield reaches this position, the additional frontal thrust does not cause lateral horizontal displacement. Since the cutter of the shield is far away from the position of synchronous grouting at the shield tail, the lateral horizontal displacement caused by synchronous grouting is small and can be almost neglected.

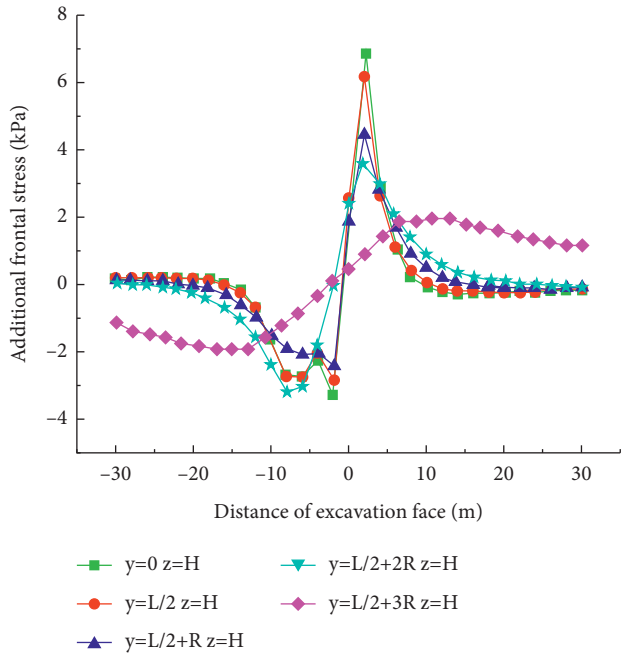

Figure 9: The distribution of the additional stress σ_y along the X axis.

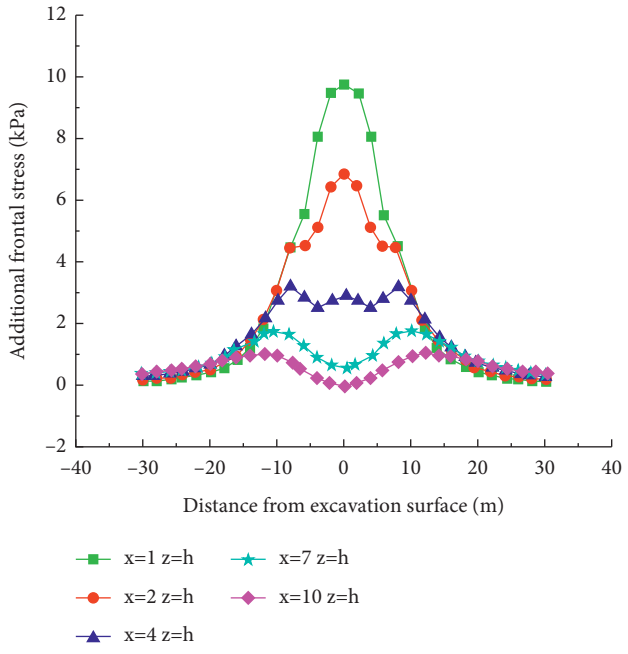

Figure 10: The distribution of the additional stress σ_y along the Y axis.

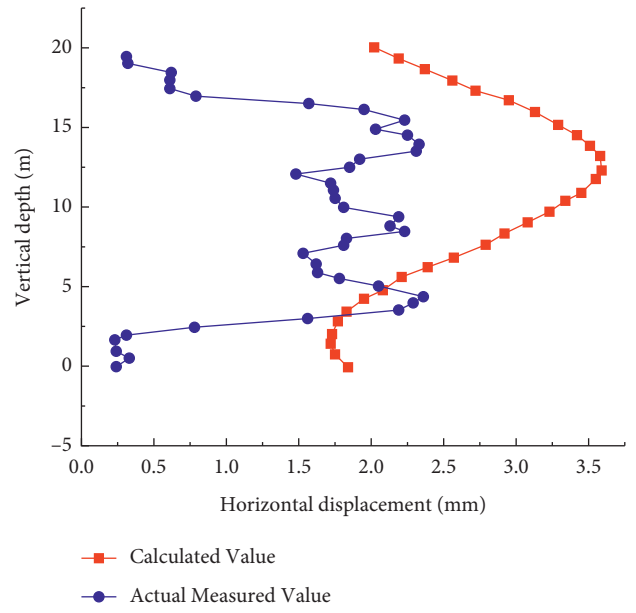

Figure 11: Comparison of calculated value and monitoring data of horizontal displacement.

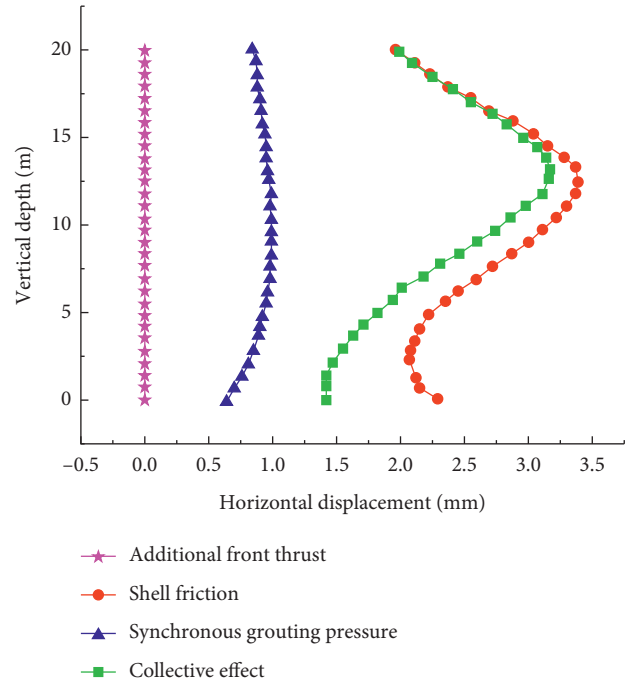

Figure 12: Horizontal deformation of the soil around the shield tunnel.

As been seen in Figure 12 that the shell frictional resistance causes a large horizontal displacement towards the outside of the tunnel, which can reach a maximum 3 mm.

6.3.3. Longitudinal Ground Deformation. The analysis results of the longitudinal deformation of the ground caused by three factors are shown in Figure 13. Under the additional frontal thrust and shell friction, the soil in front of the excavation is raised and the soil at the rear is settled, but the values are small. The peak point of surface deformation differs due to the difference in the action range. The peak point of the longitudinal deformation of the surface caused by the frontal additional stress is located roughly 5 m before and after the excavation, and the peak displacement is about 1 mm; the

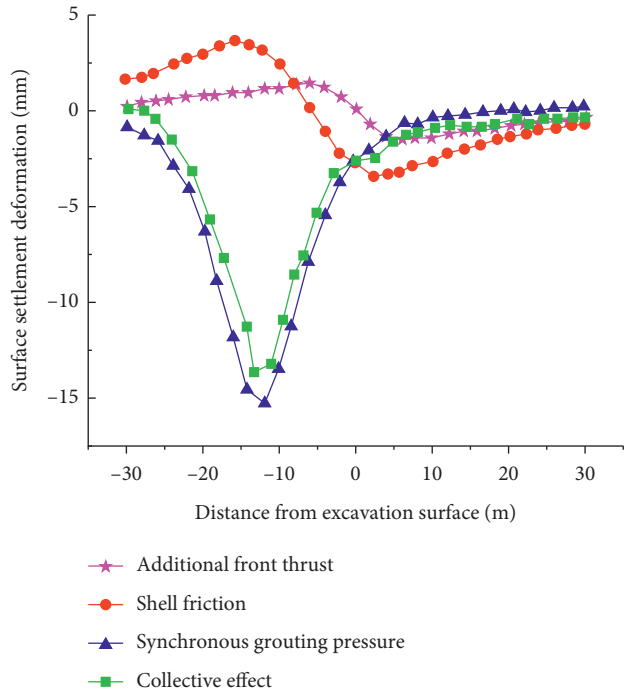

Figure 13: Longitudinal deformation of the ground surface caused by quasi-rectangle shield construction.

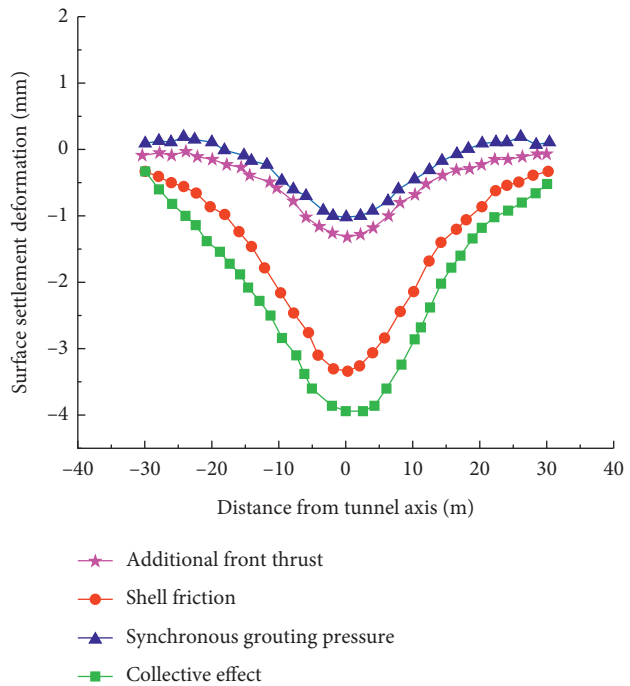

Figure 14: Lateral surface deformation of the ground surface caused by quasirectangle shield construction.

peak point of the longitudinal deformation of the surface caused by the frictional resistance of the shell is located roughly at the tail of the shield and at the face of the excavation, and the peak displacement is about 3.5 mm. The longitudinal deformation of the ground surface caused by synchronous grouting pressure causes a large bulge in the shield tail position, and the maximum value can reach 15 mm, and then rapidly spread to the front and rear of the shield tail.

6.3.4. Lateral Ground Deformation. Figure 14 illustrates the result of the lateral trough settlement caused by the three factors of frontal additional thrust, shell friction, and synchronous grouting pressure at 5 m away from the front of the shield excavation. Obviously, the lateral deformation of the surface is symmetrically distributed about the tunnel axis with an influence range of roughly 20 m on each side of the axis. The three factors have similar effects on the lateral deformation of the surface. Because this position is far from the synchronous grouting position of the shield tail, the influence of synchronous grouting factors is small, and it is close to the front additional thrust. The impact of shell friction on lateral surface deformation is large, up to 3.5 times that of the frontal additional thrust.

7. Conclusion

In this paper, based on the quasirectangular shield tunnelling of Ningbo Metro Line 3, the theoretical calculation formula is used to study the additional stress and ground deformation of the soil caused by the quasirectangle shield excavation. The following conclusions can be summarized:

(1) Based on the basic solution of the analytical stiffness matrix method, the distribution pattern of additional stress and deformation of the soil around the shield caused by the additional thrust on the frontal side of the excavation, the frictional force between the shield shell and the soil body, and the synchronous grouting pressure of the quasirectangular shield in multilayered soft soils are analyzed. The theoretical results are consistent with the monitoring data indicating that the analytical stiffness matrix method can be applied to analyze the environmental effects induced by the construction of a quasirectangular shield.

(2) The influence range of the additional stress is 25 m before and after the shield excavation, which is about 2.2 times the length of the shield, and its range along the horizontal direction of the shield is 20 m on each side of the shield axis, which is about 1.7 times the width of the shield. The farther away from the excavation surface or shield axis, the smaller the additional stress value.

(3) The shell friction and synchronous grouting pressure have a significantly greater influence on the additional stress, assuming that the shell friction and synchronous grouting pressure are uniformly distributed along the excavation surface, in most of the existing studies, a large error compared to the actual situation.

(4) The horizontal settlement curve of the quasirectangle shield is roughly symmetrical along the tunnel axis, with a groove width range of about 20 m. Case friction has a greater effect on horizontal displacement.

(5) Synchronous grouting pressure has a greater effect on longitudinal surface deformation. Synchronous grouting pressure causes a large bulge displacement in the shield tail, the maximum value of which can reach 15 mm, and then spreads rapidly to the front and back of the shield tail.

Data Availability

The data presented in this study are available in the main text of the article.

Conflicts of Interest

The authors declare that they have no conflicts of interest regarding the publication of this paper.

Acknowledgments

This work was supported by the Natural Science Foundation of China (grant no. 52079128) and Science and Technology Project of Henan Province (grant no. 212102310289).

References

[1] Y. H. Zhu, Y. F. Zhu, D. Z. Huang, and P. N. Li, "Development and application of the technical system for quasi-rectangular shield tunnelling," *Mod. Tunn. Technol*, vol. 53, no. S1, pp. 01–12, Apr. 2016.

[2] Q. Fang, J. Du, J. Li, D.-l. Zhang, and L.-q. Cao, "Settlement characteristics of large-diameter shield excavation below existing subway in close vicinity," *J. Cent. South Univ.*vol. 28, no. 3, pp. 882–897, 2021.

[3] H. Qiu, X. Zhang, and M. Daddow, "Prediction of ground settlement induced by slurry shield tunnelling in granular soils," *Civil Engineering Journal*, vol. 6, no. 12, pp. 2273–2289, 2020.

[4] X. Zhang, J. Chen, Y. Bai, A. Chen, and D.-z. Huang, "Ground surface deformation induced by quasi-rectangle EPB shield tunneling," *Journal of Zhejiang University*, vol. 52, no. 2, pp. 317–324, 2018.

[5] X. Jiang, X. Zhang, A. Chen, J. Chen, and Y. Bai, "Ground surface deformation analysis of quasi rectangular EPB shield tunneling," in *Proceedings of the GeoShanghai 2018 International Conference: Tunnelling and Underground Construction*, pp. 103–111, Springer, Singapore, 2018.

[6] G. Wei, H. Zhang, F. Xu, and Z. Wang, "Prediction of ground settlement due to excavation of a quasi-rectangular shield tunnel based on stochastic medium theory," *Geotechnical & Geological Engineering*, vol. 37, no. 5, pp. 3605–3618, 2019.

[7] W. Zhao, P.-j. Jia, L. Zhu et al., "Analysis of the additional stress and ground settlement induced by the construction of double-O-tube shield tunnels in sandy soils," *Applied Sciences*, vol. 9, no. 7, p. 1399, 2019.

[8] D. Hu, Y. Li, X. Liang, Y. Wu, S. Zhang, and Q. Yao, "Analysis and prediction of pavement settlement caused by jacking construction of ultra-shallow rectangular shield frame bridge," *Mathematical Problems in Engineering*, vol. 2020, Article ID 9624927, 14 pages, 2020.

[9] H. Li and F. Li, "Analytical solutions to ground settlement induced by ground loss and construction loadings during curved shield tunneling," *Journal of Zhejiang University - Science*, vol. 22, no. 4, pp. 296–313, 2021.

[10] S. Li, P. Li, and M. Zhang, "Analysis of additional stress for a curved shield tunnel," *Tunnelling and Underground Space Technology*, vol. 107, Article ID 103675, 2021.

[11] C. F. Wu, C. Wei, and F. F. Qiao, "Analysis of additional soil stress caused by shield construction under existing superstructure loads," *Chinese Journal of Rock Mechanics and Engineering*, vol. 37, pp. 1708–1720, 2018.

[12] B. Yuan, Z. Li, Z. Zhao, H. Ni, Z. Su, and Z. Li, "Experimental study of displacement field of layered soils surrounding laterally loaded pile based on Transparent Soil," *Journal of Soils and Sediments*, vol. 21, no. 9, pp. 3072–3083, 2021.

[13] B. Yuan, Z. Li, Y. Chen et al., "Mechanical and microstructural properties of recycling granite residual soil reinforced with glass fiber and liquid-modified polyvinyl alcohol polymer," *Chemosphere*, vol. 286, Article ID 131652, 2022.

[14] R. Liang, W. Wu, F. Yu, G. Jiang, and J. Liu, "Simplified method for evaluating shield tunnel deformation due to adjacent excavation," *Tunnelling and Underground Space Technology*, vol. 71, pp. 94–105, 2018.

[15] J. Lai, J. Qiu, Z. Feng, J.-x. Chen, and H.-b. Fan, "Prediction of soil deformation in tunnelling using artificial neural networks," *Computational Intelligence and Neuroscience*, vol. 2016, Article ID 6708183, 16 pages, 2016.

[16] Z. Zhang, M. Huang, X. Xi, and X. Yang, "Complex variable solutions for soil and liner deformation due to tunneling in clays," *International Journal of Geomechanics*, vol. 18, no. 7, Article ID 04018074, 2018.

[17] H. N. Wang, G. S. Zeng, and M. J. Jiang, "Analytical stress and displacement around non-circular tunnels in semi-infinite ground," *Applied Mathematical Modelling*, vol. 63, pp. 303–328, 2018.

[18] B. Zeng and D. Huang, "Soil deformation induced by Double-O-Tube shield tunneling with rolling based on stochastic medium theory," *Tunnelling and Underground Space Technology*, vol. 60, pp. 165–177, 2016.

[19] J. Zou and S. Zuo, "Similarity solution for the synchronous grouting of shield tunnel under the vertical non-axisymmetric displacement boundary condition," *Advances in Applied Mathematics and Mechanics*, vol. 9, no. 1, pp. 205–232, 2017.

[20] W. G. Zhang, H. R. Li, C. Z. Wu, Y. Q. Li, Z. Q. Liu, and H. L. Liu, "Soft computing approach for prediction of surface settlement induced by earth pressure balance shield tunneling," *Underground Space*, vol. 6, no. 4, pp. 353–363, 2021.

[21] L. Kou and Y. Bai, "Analytical stiffness matrixes for biot consolidation of multilayered viscoelastic foundations in the cartesian coordinate system," *Applied Mathematics and Mechanics*, vol. 37, no. 1, pp. 84–96, 2016.

[22] R. Z. Liang, T. D. Xia, C. G. Lin, and F. Yu, "Analysis of ground surface displacement and horizontal movement of deep soils induced by shield advancing," *Chinese Journal of Rock Mechanics and Engineering*, vol. 34, no. 3, pp. 583–593, 2015.

[23] C. G. Lin, Z. M. Zhang, S. M. Wu, Z.-l. Li, and G.-s. Liu, "Study of ground heave and subsidence induced by shield tunnelling in soft ground," *Chinese Journal of Rock Mechanics and Engineering*, vol. 30, no. 12, pp. 2583–2592, 2011.

[24] H. X. Wang, "Effect of cutterhead compressing the front soil and influence of head aperture ratio on contact pressure of EPB shield to the front soil," *China Civil Engineering Journal*, vol. 42, no. 7, pp. 113–118, 2009.

[25] E. E. Alonso, A. Josa, and A. Ledesma, "Negative skin friction on piles: a simplified analysis and prediction procedure," *Géotechnique*, vol. 34, no. 3, pp. 341–357, 1984.